large single crystals is encountered. Although boules several grams in weight are readily produced, Ga_2O_3 has a strong tendency to twin in the growth process. This results in samples built up of small needle-like single crystals, some of which have their b axis in one direction, and the remainder their b axis in the opposite direction. Even if large single crystals cannot be produced, it may be possible to overcome this difficulty by judicious choice of sample orientation. The possibility of using Cr^{3+} in Ga_2O_3 as the active material in an optical maser is somewhat less promising, although well worth considering. All of the required characteristics are present to some extent. The linewidth of a few Å is greater than would be desired but could possibly be reduced by almost an order of magnitude with refinements in crystal preparation techniques. Experiments to determine the factors that so strongly affect the quantum efficiency would also be required for perfecting the growth technique. However, it is significant that the quantum efficiency of the best fluorescing samples produced to date is not very different from that of ruby. Another important consideration is whether R-line light is absorbed by the excited system. Experimental investigation of this question has not been performed. On the basis of experiments completed at this time, with the sample quality presently available and the difficulty of fabricating a laser rod, it appears that the operation of this system as a laser would be marginal, at best.

ACKNOWLEDGMENTS

The author is indebted to M. Birnbaum for his efforts in initiating the program to grow Ga_2O_3 and for helpful discussions during the course of this investigation. He is especially indebted to A. Chase for growing the crystals on which most of the work was performed and for his continued interest in this program. The contribution of J. Rowen for supplying the flux grown crystals on which some of the earlier experiments were performed is gratefully acknowledged. Thanks are also due P. Kisliuk for discussions that were valuable in interpreting some of the data and to G. Wolton for his patient explanation of several aspects of the Ga_2O_3 crystal structure.

PHYSICAL REVIEW VOLUME 137, NUMBER 3A 1 FEBRUARY 1965

Electronic Band Structure of Arsenic. I. Pseudopotential Approach*

L. M. Falicov and Stuart Golin

Department of Physics and Institute for the Study of Metals, University of Chicago, Chicago, Illinois

(Received 17 August 1964)

The electronic band structure of arsenic is studied by means of a pseudopotential approach. The pseudopotential has been chosen by (a) fitting the "atomic" pseudopotential of Ge to a four-parameter curve and (b) adjusting the parameters slightly so as to allow comparison of the various theoretical curves with the experimental data. The energy bands are determined by diagonalizing a fairly large ($\approx 90 \times 90$) secular determinant. Spin-orbit coupling is included *a posteriori*. Group-theoretical analysis is carried out throughout the Brillouin zone and use is made of the classification of the levels as well as the compatibility relations. It is found that the holes are located at T, the center of the hexagonal face. The electrons are probably distributed in six equivalent pockets, each one located along a binary axis in a pseudohexagonal face, near its center L.

1. INTRODUCTION

THE group-V semimetals, As, Sb, and Bi, have been for a long time the center of interest of many investigators both from the theoretical and the experimental points of view.[1] The main reason behind this wide interest lies in the fact that a small effective number of carriers makes transport and equilibrium properties relatively easy to measure as well as easy to interpret in terms of a few parameters.

However the over-all band structure of the semimetals has remained, up to now, virtually untouched. This is so because the small number of effective carriers is in this case a drawback rather than an advantage, since only a minute region of the Brillouin zone can be reached by the standard experimental techniques. In addition the relatively low symmetry of the A7 (arsenic) structure complicates the theoretical approach. But without a reasonable overall energy-level diagram, complicated experimental measurements like optical properties[2] or behavior upon alloying[3] cannot be reliably interpreted.

Of the three group-V semimetals, arsenic is the one

* Work supported in part by the National Science Foundation and the U. S. Office of Naval Research.

[1] For a summary of the present state of the many facets of the field see, for instance, the proceedings of the Topical Conference on Semimetals, New York, IBM J. Res. Develop. 8, 215 (1964), and the many references quoted there.

[2] M. Cardona and D. L. Greenaway, Phys. Rev. 133, A1685 (1964).

[3] See Ref. 1 for work on Bi-Sb alloys and for further references.

that, because of experimental difficulties, has been studied least; on the other hand, it is the one which is most likely to be manageable from the point of view of a first-principle band structure calculation: it has the smallest atomic number ($Z=33$) and it is placed in the periodic table adjacent to germanium, for which most of the properties are well known and understood. It is then expected that the methods which give the best answers for the calculation of the band structure of Ge would give reasonable answers for As.

We have decided thus to start our study of the semimetals with arsenic, and we have computed its electronic structure by two different methods: (a) an orthogonalized-plane-wave (OPW) calculation, to be reported shortly, which is expected to achieve self-consistency, and (b) a pseudopotential approach whose results we report here.

It has been repeatedly shown[4] that the one-electron Schrödinger equation for the perfect crystal

$$[p^2/2m+V(\mathbf{r})]\psi_{n\mathbf{k}}(\mathbf{r})=E_n(\mathbf{k})\psi_{n\mathbf{k}}(\mathbf{r}) \qquad (1.1)$$

can be rewritten

$$[p^2/2m+V_p]\varphi_{n\mathbf{k}}(\mathbf{r})=E_n(\mathbf{k})\varphi_{n\mathbf{k}}(\mathbf{r}), \qquad (1.2)$$

where (1.1) and (1.2) have the same set of eigenvalues. V_p is a nonlocal integral operator, and $\varphi_{n\mathbf{k}}$ is a smooth function which does not include the typical atomic-core oscillation of the real wave function $\psi_{n\mathbf{k}}$. Consequently an expansion in plane waves of $\varphi_{n\mathbf{k}}$ is free of the slow-convergence difficulties that the corresponding expansion of $\psi_{n\mathbf{k}}$ is known to have.

The matrix elements of V_p between plane waves of wave vectors $\mathbf{k}$ and $\mathbf{k}'$ are nonzero only when

$$\mathbf{k}-\mathbf{k}'=\mathbf{G}, \qquad (1.3)$$

where $\mathbf{G}$ is a reciprocal lattice vector; in general these matrix elements depend on $\mathbf{k}$ as well as on $\mathbf{G}$. However, as it has been proved for the case of silicon and germanium,[5,6] quantitative agreement with experiment can be obtained even if two greatly simplifying assumptions are made: (i) V_p is expressed as a superposition of atomic-like pseudopotentials centered about each ion site

$$V_p=\sum_{\alpha,\ \text{ion sites}} U_\alpha; \qquad (1.4)$$

(ii) the atomic like pseudopotentials are local, i.e., they are simple (spherically symmetric) functions of position rather than integral operators:

$$U_\alpha=U(|\mathbf{r}-\mathbf{r}_\alpha|). \qquad (1.5)$$

Under these circumstances the matrix elements of the pseudopotential can be decomposed into a product of a structure factor $S(\mathbf{G})$ and the Fourier transform $U(\kappa)$ of the atomic-like pseudopotential, taken at the value $\kappa=|\mathbf{G}|=|\mathbf{k}-\mathbf{k}'|$.

In this fashion a band structure can be specified by a simple function $U(\kappa)$, the Fourier transform of the "atomic" pseudopotential, or more simply, by the set of numbers $\{U(|\mathbf{G}|)\}$.

Brust has proved[6] by actual computations, that quantitative agreement with experiment as well as with more sophisticated band structure calculations can be achieved for Ge or Si with only three nonvanishing $U(|\mathbf{G}|)$.

As a first approximation in our calculation, we drew a smooth curve through the points determined by Brust for Ge; in this way we selected a function $U(\kappa)$ which, included in a band calculation with the lattice parameters and structure factors of As, yielded, surprisingly enough, a semimetallic structure. In addition this structure was very similar to preliminary results of the orthogonalized-plane-wave calculations. The encouraging results of this first approach pointed out that for "reasonable" atomic pseudopotentials, most of the qualitative features of the energy bands are in fact implicit in the crystal structure,[7] and that, hopefully, quantitative agreement with experiment could be obtained by slight readjustments of the atomic pseudopotential.

In Sec. 2 we discuss the As crystal structure, its departure from the simple-cubic and face-centered-cubic symmetries and the determination of the structure factors. Section 3 is devoted to the group-theoretical properties of the energy bands, i.e., the representations at points and lines of symmetry in the Brillouin zone as well as the compatibility relations. The actual choice of the "atomic" pseudopotential and the mechanics of the calculations are described in Sec. 4. Section 5 gives the results and makes a comparison with experiment. In Sec. 6 the influence of spin-orbit coupling is discussed.

We use atomic units throughout, i.e., the numerical values of m, $\hbar$, and e are one, the unit of length is one Bohr radius $a_0=0.529$ Å and the unit of energy is 1 hartree $=2$ Ry $=27.2$ eV.

2. THE CRYSTAL STRUCTURE OF As AND THE STRUCTURE DEPENDENCE OF THE PSEUDOPOTENTIAL

Crystal Structure

The group-V semimetals, As, Sb, and Bi, all have the A7 (arsenic) crystal structure.[8] The unit cell (which is also a primitive cell) is rhombohedral and contains 2 atoms.

The A7 structure can be obtained from a simple-cubic

[4] J. C. Phillips and L. Kleinman, Phys. Rev. **116**, 287 (1959); M. H. Cohen and V. Heine, *ibid.* **122**, 1821 (1961); B. J. Austin, V. Heine, and L. J. Sham, *ibid.* **127**, 276 (1962).
[5] J. C. Phillips and L. Kleinman, Phys. Rev. **128**, 2098 (1962).
[6] D. Brust, Phys. Rev. **134**, A1337 (1964).
[7] For a detailed analysis of the relation between structure and semimetallic character see M. H. Cohen, L. M. Falicov, and S. Golin, IBM J. Res. Develop. **8**, 215 (1964).
[8] R. W. G. Wyckoff, *Crystal Structures* (Interscience Publishers, Inc., New York, 1960), Vol. 1.

structure with one atom at each lattice site by applying two independent distortions: a shear and an internal displacement of the atoms. The shear is along a body diagonal and transforms the unit cube into a rhombohedron. This diagonal retains its 3-fold symmetry and becomes the trigonal axis of the A7 structure. To visualize the 2nd distortion, it is convenient to think of the simple-rhombohedral lattice as being composed of two interpenetrating face-centered-rhombohedral lattices. Each point of either lattice is in the center of the cell of the other lattice. Then the A7 structure is obtained by shifting one of these lattices toward the other along the trigonal axis. This results in a face-centered-rhombohedral structure in which 2 atoms are associated with each lattice point.

Two parameters are needed to specify these distortions:

(a) The parameter u is used to characterize the internal displacement. If $2\boldsymbol{\tau}$ is the (smaller) vector in the trigonal direction separating the two interpenetrating lattices, and $\mathbf{d}$ is the trigonal body-diagonal of one of the lattices, then

$$\boldsymbol{\tau}=u\mathbf{d};\quad u\leqslant\tfrac{1}{4}. \tag{2.1}$$

The value $u=\frac{1}{4}$ corresponds to a simple-rhombohedral structure or to a simple-cubic structure in the absence of shear; $u=\frac{1}{8}$ and no shear correspond to the diamond structure.

(b) The angle α between the primitive translations of the A7 structure determines the shear, 60° being the value corresponding to the face-centered cubic (or simple-cubic) structures.

Table I and Appendix A give a more detailed account of the crystal structure parameters of arsenic; Fig. 1 shows the Brillouin zone with its points, lines, and planes of symmetry. We have followed Cohen's[9] notation for points and lines of symmetry.

One feature of the structure is worth mentioning at this point. The internal displacement of the two atoms in the unit cell destroys the inversion centers at the atom sites. However, the points midway between two adjacent atoms along the trigonal direction, which were the cubic centers before the distortions, remain centers of inversion. It is thus convenient to choose one of these points as the origin of the coordinate system and the center of the unit cell. In this way the structure factors turn out to be real; i.e.,

$$S(\mathbf{G})=\tfrac{1}{2}\sum_{j,\text{ unit cell}}\exp(i\mathbf{G}\cdot\mathbf{r}_j)=\cos(\mathbf{G}\cdot\boldsymbol{\tau}). \tag{2.2}$$

In (2.2) $\mathbf{r}_j$ denotes the position of the atoms in the unit cell and the factor $\frac{1}{2}$ was included for convenience.

TABLE I. Crystal structure parameters for arsenic.

Symbol	Value (atomic units)	Definitions and remarks
$\lvert a_i\rvert$	7.807	Lattice parameter; room temperature[a]
α	54° 10′	Rhombohedral angle; room temperature[a]
u	0.226	Internal displacement parameter; room temperature[a]
$\lvert\boldsymbol{\tau}\rvert$	4.502	Half the minimum distance between atoms along trigonal direction
Ω_0	290.7	Volume of the unit cell
$(2\pi)^3/\Omega_0$	0.8533	Volume of the Brillouin zone
k_F	1.006	Free-electron Fermi momentum
E_F	0.518	Free-electron Fermi energy
a_0	5.510	See Appendix A
g_0	0.5987	See Appendix A
ϵ	0.0877	See Appendix A

[a] See Ref. 8.

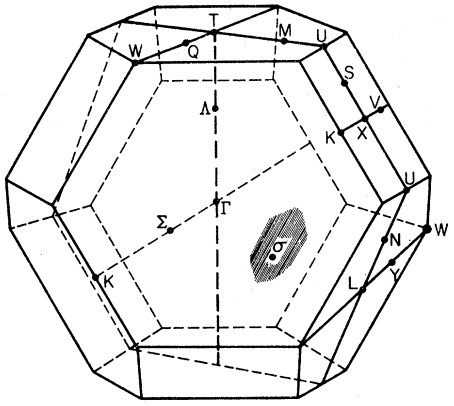

FIG. 1. The Brillouin zone for the arsenic A7 structure showing points and lines of symmetry.

Pseudopotential

If the crystal pseudopotential V_p is assumed to be a superposition of local atomic pseudopotentials, its matrix element between two plane waves takes the form

$$\langle\mathbf{k}|V_p|\mathbf{k}'\rangle=S(\mathbf{G})U(|\mathbf{G}|), \tag{2.3}$$

where $\mathbf{G}=\mathbf{k}-\mathbf{k}'$ is a reciprocal lattice vector and $S(\mathbf{G})$ is the structure factor (2.2). $U(|\mathbf{G}|)$ is the Fourier transform $U(\kappa)$ of the atomic pseudopotential (which is a smooth function of its argument) taken at $\kappa=|\mathbf{G}|$.

The structure factor for a given $\mathbf{G}$ depends only on the internal displacement parameter u, and is independent of the shear. In fact if

$$\mathbf{G}=[h,k,l]\equiv h\mathbf{g}_1+k\mathbf{g}_2+l\mathbf{g}_3, \tag{2.4}$$

where the $\mathbf{g}_i$ are the primitive reciprocal lattice vectors as defined in Appendix A, and hkl are integers, it follows that

$$S(\mathbf{G})=\cos(\mathbf{G}\cdot\boldsymbol{\tau})=\cos[2\pi u(h+k+l)]. \tag{2.5}$$

When $u=\frac{1}{4}$ (simple-rhombohedral structure) or $\frac{1}{8}$ (diamond structure), the structure factor, and hence the matrix elements, will vanish for many reciprocal lattice vectors. For the semimetals, u is irrational and

[9] M. H. Cohen, Phys. Rev. **121**, 387 (1961).

$S(\mathbf{G})$ does not vanish. Thus the value of u has a profound effect on $S(\mathbf{G})$ and ultimately on the band structure.[7]

$U(|\mathbf{G}|)$ on the other hand is independent of u. It depends on shear only in the sense that it determines the values $\kappa=|G|$ at which the function $U(\kappa)$ must be evaluated. Since U is a "smooth" function, we expect that the matrix elements will not be greatly altered by the shear.[7]

The shear however has a profound influence on the kinetic energy terms; by changing the length of the reciprocal lattice vectors it changes the relative kinetic energy of some symmetry points with respect to others. At values close to the Fermi energy the shift of T with respect to L for instance is of the order of 0.03 hartree ($\sim$1 eV).[7] The internal displacement does not affect the kinetic energy at all.

3. GROUP-THEORETICAL CONSIDERATIONS

The arsenic structure A7 corresponds to the space group $R\bar{3}m$; the point group symmetry $\bar{3}m$ (or D_{3d}) consists of 12 operations:

E	the identity,
$C_3C_3^{-1}$	rotations of 120° and 240° about the trigonal axis,
$C_{2a}C_{2b}C_{2c}$	three twofold rotations about axes perpendicular to the trigonal,
J	the inversion,
$JC_3JC_3^{-1}$	two rotation inversions by 120° and 240°,
$m_am_bm_c$	three reflection planes perpendicular to the binary axes.

The symmetry properties of the various symmetry points in the Brillouin zone (Fig. 1) have been studied by several authors.[9–11] However, for the sake of completeness as well as consistency in notation we give here the characters of the small-group representations for both the single (without spin) and double (with spin) groups. Table II gives the various representations for Γ and T, which have the full $\bar{3}m$ symmetry; Table III

TABLE II. Characters of the small-group representations of Γ and T.[a]

		E	$2C_3$	$3C_2$	J	$2JC_3$	$3m$	$R\times\bar{E}$
Γ_1	T_1	1	1	1	1	1	1	$\chi(R)$
Γ_1'	T_1'	1	1	1	−1	−1	−1	$\chi(R)$
Γ_2	T_2	1	1	−1	1	1	−1	$\chi(R)$
Γ_2'	T_2'	1	1	−1	−1	−1	1	$\chi(R)$
Γ_3	T_3	2	−1	0	2	−1	0	$\chi(R)$
Γ_3'	T_3'	2	−1	0	−2	1	0	$\chi(R)$
Γ_4^+	T_4^+	1	−1	i	1	−1	i	$-\chi(R)$
Γ_5^+	T_5^+	1	−1	$-i$	1	−1	$-i$	$-\chi(R)$
Γ_6^+	T_6^+	2	1	0	2	1	0	$-\chi(R)$
Γ_4^-	T_4^-	1	−1	i	−1	1	$-i$	$-\chi(R)$
Γ_5^-	T_5^-	1	−1	$-i$	−1	1	i	$-\chi(R)$
Γ_6^-	T_6^-	2	1	0	−2	−1	0	$-\chi(R)$

[a] Representations degenerate by time-reversal symmetry are connected by braces.

$$\times D^{1/2}=\begin{matrix}T_1 & T_1' & T_2 & T_2' & T_3 & T_3'\\ T_6^+ & T_6^- & T_6^+ & T_6^- & T_4^++T_5^++T_6^+ & T_4^-+T_5^-+T_6^-\end{matrix}$$

and similarly for Γ.

TABLE III. Characters of the small-group representations of Λ.[a]

	E	$2C_3$	$3m$	$R\times\bar{E}$
Λ_1	1	1	1	$\chi(R)$
Λ_2	1	1	−1	$\chi(R)$
Λ_3	2	−1	0	$\chi(R)$
Λ_4	1	−1	i	$-\chi(R)$
Λ_5	1	−1	$-i$	$-\chi(R)$
Λ_6	2	1	0	$-\chi(R)$

[a] Representations degenerate by time-reversal symmetry are connected by braces

$$\times D^{1/2}=\begin{matrix}\Lambda_1 & \Lambda_2 & \Lambda_3\\ \Lambda_6 & \Lambda_6 & \Lambda_4+\Lambda_5+\Lambda_6\end{matrix}.$$

TABLE IV. Characters of the small-group representations of X and L.[a]

		E	C_2	J	m	$R\times\bar{E}$
X_1	L_1	1	1	1	1	$\chi(R)$
X_2	L_2	1	−1	1	−1	$\chi(R)$
X_3	L_3	1	1	−1	−1	$\chi(R)$
X_4	L_4	1	−1	−1	1	$\chi(R)$
X_5	L_5	1	i	1	i	$-\chi(R)$
X_6	L_6	1	$-i$	1	$-i$	$-\chi(R)$
X_7	L_7	1	i	−1	$-i$	$-\chi(R)$
X_8	L_8	1	$-i$	−1	i	$-\chi(R)$

[a] Representations degenerate by time-reversal symmetry are connected by braces

$$\times D^{1/2}=\begin{matrix}L_1 & L_2 & L_3 & L_4\\ L_5+L_6 & L_5+L_6 & L_7+L_8 & L_7+L_8\end{matrix}$$

and similarly for X.

TABLE V. Characters of the small-group representations of points along the binary axis.[a]

	E	C_2	$R\times\bar{E}$
W_1	1	1	$\chi(R)$
W_2	1	−1	$\chi(R)$
W_3	1	i	$-\chi(R)$
W_4	1	$-i$	$-\chi(R)$

[a] Representations degenerate by time-reversal symmetry are connected by braces

$$\times D^{1/2}=\begin{matrix}W_1 & W_2\\ W_3+W_4 & W_3+W_4\end{matrix}$$

and similarly for K, Σ, Q, Y, and V.

TABLE VI. Characters of the small-group representations of points in the reflection planes.[a]

	E	m	$R\times\bar{E}$
U_1	1	1	$\chi(R)$
U_2	1	−1	$\chi(R)$
U_3	1	i	$-\chi(R)$
U_4	1	$-i$	$-\chi(R)$

[a] Representations degenerate by time-reversal symmetry are connected by braces

$$\times D^{1/2}=\begin{matrix}U_1 & U_2\\ U_3+U_4 & U_3+U_4\end{matrix}$$

and similarly for σ, M, S, and N.

[10] S. Mase, J. Phys. Soc. Japan **13**, 434 (1958); **14**, 584 (1959).
[11] A. A. Abrikosov and L. A. Falkovskii, Zh. Eksperim. i Teor. Fiz. **43**, 1089 (1962) [English transl.: Soviet Phys.—JETP **16**, 769 (1963)].

gives the representations for the Λ line which has $3m$ symmetry; Table IV shows the representations for X and L, with $2/m$ symmetry; Tables V and VI give the characters for the representations at points along binary axes and on reflection planes, respectively.

The compatibility relations between points of symmetry along lines and planes of symmetry are shown in Table VII; they are of fundamental importance in

TABLE VII. Compatibility relations between points of symmetry along the various symmetry lines and planes.

1st symmetry point				Connecting representation	2nd symmetry point			
	Γ_1		Γ_2'	Λ_1		T_1		T_2'
	Γ_1'		Γ_2	Λ_2		T_1'		T_2
	Γ_3		Γ_3'	Λ_3		T_3		T_3'
Γ_1	Γ_1'	Γ_3	Γ_3'	Σ_1			K_1	
Γ_2	Γ_2'	Γ_3	Γ_3'	Σ_2			K_2	
Γ_1	Γ_2'	Γ_3	Γ_3'	σ_1	X_1	X_4	L_1	L_4
Γ_1'	Γ_2	Γ_3	Γ_3'	σ_2	X_2	X_3	L_2	L_3
T_1	T_1'	T_3	T_3'	Q_1			W_1	
T_2	T_2'	T_3	T_3'	Q_2			W_2	
T_1	T_2'	T_3	T_3'	M_1			U_1	
T_1'	T_2	T_3	T_3'	M_2			U_2	
X_1	X_4	L_1	L_4	S_1 or N_1			U_1	
X_2	X_3	L_2	L_3	S_2 or N_2			U_2	
	X_1		X_3	V_1			K_1	
	X_2		X_4	V_2			K_2	
	L_1		L_3	Y_1			W_1	
	L_2		L_4	Y_2			W_2	

determining points of accidental degeneracy as well as a tool for connecting the various energy levels obtained numerically at different points.

4. THE CHOICE OF THE PSEUDOPOTENTIAL AND THE MECHANICS OF THE CALCULATION

The choice of $U(\kappa)$, the Fourier transform of the "atomic" pseudopotential was made in two parts: (a) by passing a smooth curve through the four points determined by Brust[6] for Ge; (b) by representing that curve by a four-parameter analytic expression and slightly varying the parameters. Figure 2 shows the values given by Brust and the interpolation by means of the function

$$U(\kappa)=A_1(\kappa^2-A_2)[\exp A_3(\kappa^2-A_4)+1]^{-1}. \quad (4.1)$$

The fitting parameters were found to be

$$A_1=0.0655, \quad A_2=2.78,$$
$$A_3=2.38, \quad A_4=3.70; \quad (4.2)$$

the corresponding pseudopotential was designated $P1$. The choice of the analytic form (4.1) has no deeper meaning than a convenient interpolation formula which permits one, by adjusting only four parameters, to obtain a fairly accurate fit of the band structure to experimental data.

The solution of the Schrödinger equation (1.2) was

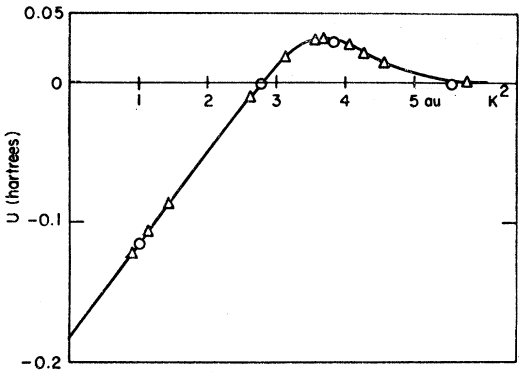

FIG. 2. The pseudopotential $P1$. The circles indicate the values given by Brust (Ref. 6) for Ge. The solid line is the analytic curve given by formulas (4.1) and (4.2) and the triangles give the values $U(|\mathbf{G}|)$ actually taken in the calculation.

accomplished by expanding $\varphi_{n\mathbf{k}}$ in a series of symmetrized combinations of plane waves, calculating the matrix elements of the Hamiltonian, and solving the corresponding secular equation. The smooth part of the wave function is thus expanded

$$\varphi_{n\mathbf{k}}(\mathbf{r})=\sum_m b_m{}^n L_{m\mathbf{k}}, \quad (4.3)$$

where

$$L_{m\mathbf{k}}=\Omega^{-1/2}\sum_j a_{mj}\exp[i(\mathbf{k}-\mathbf{G}_{mj})\cdot\mathbf{r}]. \quad (4.4)$$

In (4.4) Ω is the volume of the crystal and the $\mathbf{G}_{mj}$ are reciprocal lattice vectors. The set of vectors $\mathbf{k}-\mathbf{G}_{mj}$, for the same m and $\mathbf{k}$, all have the same magnitude and are related to each other by operations of the small group of $\mathbf{k}$. The coefficients a_{mj} of the symmetrized combinations $L_{m\mathbf{k}}$ were calculated by means of the character tables of Sec. 3; some of them are listed in Appendix B.

Substitution of (4.3) and (4.4) into (2.1) leads to

$$\sum_m b_m{}^n H_{pm}(\mathbf{k})=E_{n\mathbf{k}}b_p{}^n, \quad (4.5)$$

where

$$H_{pm}(\mathbf{k})=\tfrac{1}{2}|\mathbf{k}-\mathbf{G}_{mi}|^2\delta_{pm}+\sum_{ij} a_{mi}{}^* a_{pj}$$
$$\times\cos[(\mathbf{G}_{mi}-\mathbf{G}_{pj})\cdot\boldsymbol{\tau}]U(|\mathbf{G}_{mi}-\mathbf{G}_{pj}|). \quad (4.6)$$

Equation (4.5) leads to the usual secular equation

$$|H_{pm}(\mathbf{k})-E_{n\mathbf{k}}\delta_{pm}|=0. \quad (4.7)$$

The solution of (4.7) was found numerically, by truncating the secular equation at a finite number of terms. The size of the determinant depended on the symmetry of the small group of $\mathbf{k}$; in the actual cases computed it varied from a 12×12 at Γ and T to a 54×54 for points on the reflection plane and 89×89 when no symmetry was taken into account. The

TABLE VIII. Energy levels for various pseudopotentials.

Designation	A_1	A_2	A_3	A_4	X_1	L_1	L_1	L_4	T_1	T_3
$P1$	0.0655	2.78	2.38	3.70	0.55943	0.52880	0.53134	0.53981	0.55954	0.57039
$P2$	0.0600	2.78	2.38	3.70	0.56876	0.54436	0.55649	0.55871	0.58047	0.59151
$P3$	0.0550	2.78	2.38	3.70	0.57658	0.55772	0.57915	0.57570	0.59938	0.60953
$P4$	0.0655	2.60	2.38	3.70	0.55924	0.53834	0.56265	0.56790	0.60378	0.57982
$P5$	0.0655	2.40	2.38	3.70	0.55840	0.54449	0.59655	0.59705	0.64638	0.58730
$P6$	0.0655	2.78	2.20	3.70	0.55980	0.52899	0.53104	0.54072	0.56137	0.57043
$P7$	0.0655	2.78	2.00	3.70	0.56011	0.52939	0.53083	0.54186	0.56369	0.57054
$P8$	0.0655	2.78	2.38	3.40	0.55878	0.52448	0.54237	0.52953	0.53747	0.57508
$P9$	0.0655	2.78	2.38	3.10	0.55796	0.52111	0.55038	0.52081	0.51954	0.58018

calculations were carried out on the IBM 7094 system of the University of Chicago Computation Center.

5. RESULTS OF THE CALCULATIONS AND COMPARISON WITH EXPERIMENT

Energy levels at various points of the Brillouin zone, obtained through calculations with several pseudopotentials, are shown in Table VIII. The over-all structure of the bands is essentially unchanged for all nine cases; a few level crossings can be observed, but the general features are quite similar throughout. This reflects the facts that (a) the kinetic energy term of the Hamiltonian is more important than the pseudopotential term, and (b) the structure factor in the pseudopotential matrix elements (2.3) dominate for any "reasonable" variation of the atomic-like factor.

Figure 3 shows the band structure obtained for pseudopotential $P1$. The approximate position of the Fermi energy is indicated, and it can be seen that only the energy bands near L and T cross the Fermi level. This means that, on the whole, five bands are doubly occupied throughout, except close to L, where some "electrons" are in the sixth band, and close to T, where "holes" are left in the fifth band.

In order to compare these results with experiment, it is useful at this stage to summarize the available experimental information. As far as we are aware, there are as of today only two sets of experimental data which yield information on the band structure of As. These are the optical reflectivity measurements of Cardona and Greenaway[2] and the de Haas–van Alphen (dH–vA) measurements of Berlincourt.[12] The interpretation of the optical data requires extensive computations[6] which we expect to carry out in the not too distant future. We therefore restrict ourselves to the dH–vA data. The measurements of Berlincourt[12] show several oscillations due to different sets of carriers, which will be described in turn.

Electrons

A first set of carriers, presumably electrons, are distributed in either three or six equivalent pockets. Each of these pockets shows either reflection symmetry in a plane perpendicular to a binary axis, or twofold rotational symmetry about a binary axis, or both. This kind of symmetry is found also in the "electrons" in antimony and bismuth.

If the electron pockets are only three, symmetry requires them to be at either L or X and consequently to possess both reflection and binary-rotation symmetry. If, on the other hand, the pockets are six they may lie anywhere along binary axes (Σ, V, Y, Q, W) or on reflection planes (σ, M, U, S, N).

Berlincourt[12] interpreted his experiment by assuming that the electron pockets are ellipsoids with one principal axis parallel to a binary axis and a second principal axis normal to it and making a "tilt angle" of about 36° with the trigonal axis.

Under the following three assumptions: (a) the pockets are ellipsoidal, (b) the bands are parabolic, and (c) k vectors and energies are measured from the minimum of the band, the energy can be expressed by

$$2E=\alpha_1 k_1^2+\alpha_2 k_2^2+\alpha_3 k_3^2, \tag{5.1}$$

where k_1, k_2, and k_3 are in the directions of the principal axes of the ellipsoid. The parameters α can be interpreted as reciprocal effective masses. For the sake of definiteness we take k_1 in the binary direction, choose k_2 and k_3 so that $\alpha_2>\alpha_3$ and define the "tilt" angle θ_T as the angle between the trigonal and the k_3 axes. θ_T is positive if the k_3 axis is obtained by rotating from the $\Gamma-T$ line towards the $\Gamma-X$ line, and negative if the rotation is from $\Gamma-T$ towards $\Gamma-L$.[13,14]

With these assumptions and conventions, a complete set of measurements of dH-vA periods gives, if the Fermi energy E_F is known, the three binary products $\alpha_i\alpha_j (i\neq j)$ directly. Berlincourt's data give only $\alpha_1\alpha_2$ and θ_T unambiguously. Since in arsenic $\alpha_1>\alpha_3$, $\alpha_1\alpha_2$, and θ_T are given by measurements at the direction of magnetic field for which a maximum dH–vA period is found or, what is equivalent, the direction at which the ellipsoid itself is "pointing."

If the pockets are nonellipsoidal, the definitions given

[12] T. G. Berlincourt, Phys. Rev. **99**, 1716 (1955).

[13] The sign of the tilt angle θ_T in all the semimetals is of great importance when comparing theory with experiment; unfortunately it is tedious to measure it, and many times it has been ignored. Our definition corresponds to the convention used by Shoenberg (Ref. 14) to measure directions of magnetic fields.

[14] D. Shoenberg, Phil. Trans. Roy. Soc. (London) **245**, 1 (1952).

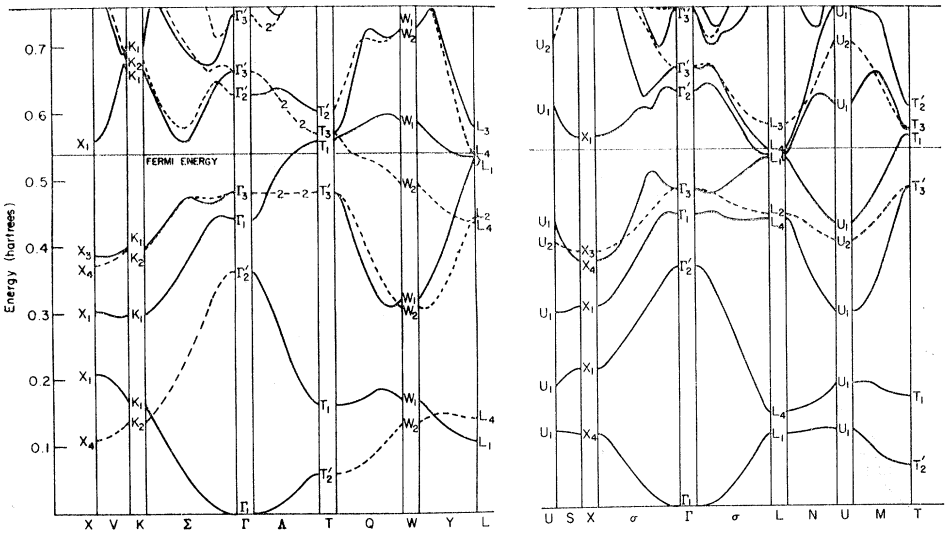

FIG. 3. The band structures of As without spin, along various symmetry lines for pseudopotential $P1$. Full lines and dotted lines indicate different symmetries; full lines correspond in each case to the fully symmetric representation. The doubly degenerate level Λ_3 is indicated by a number 2 inserted along the line.

so far lose their meaning. In particular θ_T may be defined in several ways. We choose to define it as the angle between the trigonal axis and the direction of maximum radius vector (i.e., the vector between the position of the minimum of the band and the pocket surface) normal to the binary axis. In pictorial terms, it is the direction at which the pocket is "pointing." This is in general no longer the direction of the maximum dH–vA period and, due to additional terms in the right-hand side of (5.1), $\alpha_1\alpha_2$ is no longer given by the maximum period either.

The theoretical band structure corresponding to pseudopotential $P1$ (Fig. 3) gives electrons near L, but the actual band minimum is in fact at a point along the L-W line, as shown in Fig. 4(a). This minimum along the L-W line is more pronounced for other pseudopotentials [see, for instance, Fig. 4(c) and $P8$], when the two L_1 levels near the Fermi energy are not so close to each other. The closeness of these two levels is accidental and occurs only for $P1$; other pseudopotentials (see Table VIII) and the preliminary OPW calculation do not exhibit this peculiarity.

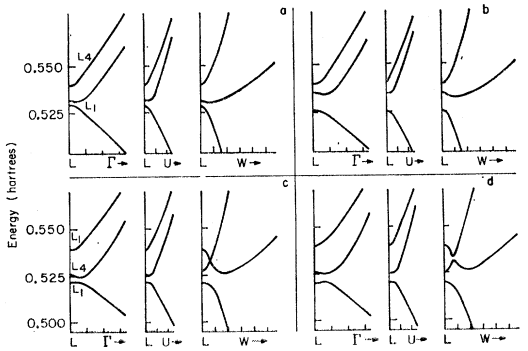

FIG. 4. Details of the band structure close to L (electrons). (a) Pseudopotential $P1$ without spin; (b) pseudopotential $P1$ with spin-orbit coupling included; (c) pseudopotential $P8$ without spin; (d) pseudopotential $P8$ with spin-orbit effects. The divisions in the abscissae indicate 1/10 of the distance between L and the corresponding end point (Γ, U, or W).

If in addition to one of the L_1 levels there is another level below the Fermi energy, there will be three electron pockets centered about the three equivalent L points. If, on the other hand, only one level (L_1) lies below the Fermi energy, there will be six equivalent electron pockets centered about equivalent points along the L-W line.

Since we believe this latter possibility to be the most likely, we shall now describe it in some detail. At the minimum (and all throughout the neighborhood of the L point) the energy difference between successive bands is very small and of the same order of magnitude as the difference between the Fermi energy and the bottom of the sixth band. Under these conditions the sixth energy band can be expected to be nonparabolic and the pockets to be nonellipsoidal. At the same time, small changes in the pseudopotential may cause large changes in the band gaps and the band parameters; these changes even result in levels crossing each other and producing different orderings. Thus the properties of the pockets are expected to be strongly dependent on the pseudopotential.

Detailed calculations show that the energy band along the direction of the binary axis (L-W line) is indeed quite sensitive to small changes in the pseudopotential and the minimum is highly nonparabolic. Thus the mass parameter α_1 along the binary is not at all well defined. However, in directions perpendicular to the binary the band is reasonably parabolic and much less dependent on small changes in the pseudopotential. Perpendicular inverse masses are at the same time reasonably well defined, i.e., α_2, α_3, and θ_T are relatively insensitive to the particular pseudopotential used (see Table IX).

TABLE IX. Reciprocal effective masses at various symmetry points.

	Location	$\alpha_1\alpha_2$	α_1	α_2	α_3	θ_T
Exp[b]	?	115	5.2	22.1	0.4	−36°
(OPW)	X_1	53.3	9.0	6.0	0.8	+49.6°
*P*1	X_1	20.4	6.7	3.1	0.83	+49.6°
(OPW)	L_4[c]	···	19.8	···	···	···
*P*1	L_4[c]	···	12.6	···	···	···
*P*8	L_4[c]	···	19.5	···	···	···
(OPW)	0.2[a]	135	6.8	19.9	1.5	−58.0°
*P*1	0.1[a]	28.7	2.9	13.2	1.0	−57.2°
*P*2	0.11[a]	167	9.6	17.4	0.5	−54.4°
*P*4	0.16[a]	76	4.7	16.1	1.2	−56.1°
*P*8	0.17[a]	110	6	17.9	0.8	−55.8°
*P*1	0.57[d]	···	4.3	···	···	···

[a] These points are along the *LW* line. The number gives the fractional distance of the point from *L* toward *W*.
[b] Assuming ellipsoidal approximation. See Ref. 15.
[c] The perpendicular masses at L_4 are poorly defined. The tilt angle may consequently take almost any value.
[d] This point is along the Γ*K* line. The number gives the fractional distance of the point from Γ towards *K*.

When the L_4 level lies between the two L_1 levels, the compatibility relations produce an intersection of levels of different symmetry along the *L*-*W* line [Fig. 4(c), for instance]; the bands near the intersection are highly nonparabolic in the directions perpendicular to the binary. Nevertheless, this behavior near the intersection has little effect on the tilt angle. In fact, calculations of constant energy surfaces near the crossover show that the tilt angle (which gives the direction at which the pocket is "pointing") is still determined quite well by the "transverse masses" at the bottom of the pocket. However the warping of these surfaces can cause a discrepancy of 20–30° between the tilt angle as defined here and the direction of maximum period of dH–vA oscillations normal to the binary axis.

Table IX lists Berlincourt's[12] (reciprocal) masses[15] and tilt angle. Listed for comparison are the theoretical masses for various pseudopotentials and from our preliminary OPW calculation at the *L*-*W* minimum and at several other band minima; the tilt angles were computed from these masses.

The masses at the *L*-*W* minimum agree reasonably well with experiment. Some of the pseudopotentials give better agreement than others, but we did not try to determine a final pseudopotential accurately. The amount of experimental evidence is very limited and comparison with the available dH–vA data becomes difficult and not very convincing when the pockets are appreciably nonellipsoidal. The tilt angle, as determined from theory, cannot be changed by more than a few degrees by varying the pseudopotential. We ascribe the rather large discrepancy with the experimental tilt angle to nonellipsoidal effects.

There are other energy levels which should be mentioned as possible sources of electron pockets. They are close to the Fermi energy and have the required symmetry.

(a) The sixth level at $X(X_1)$ would give three equivalent ellipsoids. The band is parabolic and thus the masses are well defined. We were unable to bring this level below the Fermi energy by small changes of the pseudopotential. Also there is a considerable discrepancy with experiment in the tilt angle, unless there is an error in the experimental determination of its sign.

(b) The L_4 level would give three equivalent pockets. The band is parabolic in the binary direction, but the pocket is very warped perpendicular to the binary. The tilt angle is poorly defined and can take almost any value. The binary mass differs considerably from the experimental value, but we are not sure that this suffices to discard this level.

(c) There is a minimum along the Γ-*K* line which would give six equivalent pockets. The band is parabolic in the binary direction but is very complicated in perpendicular directions.

Before the location of the electrons in the Brillouin zone can be exactly determined, more experimental information (similar in many instances to some already available for the other semimetals) is needed. It would be very helpful indeed to know the exact number of equivalent pockets (3 or 6). This determination is quite difficult when the pockets are nonellipsoidal: a considerable amount of experimental information was needed before Jain and Koenig[16] were able to set the number of electron pockets in bismuth at three.

The addition through impurities of a *known* number of conduction[17] electrons to arsenic, could confirm or reject the hypothesis that the electrons are located in six equivalent pockets at the *L*-*W* minima. Adding electrons will eventually raise the Fermi energy above the upper L_1 (or L_4) level and thus reduce the number of pockets to three. This discontinuous change in the topology from six pseudoellipsoids to three dumbbell-shaped pockets should be easily observed.

Experiments measuring nonellipsoidal and nonparabolic effects[17,18] could be quite useful. The observation of such effects would rule out *X* as the possible location of the electrons. The measurements would also allow the determination of the symmetry (binary, reflection or both) of the electron pockets.[9]

Geometric resonance experiments using ultrasonic attenuation, which measure linear dimensions of the Fermi surface directly, would be especially interesting in determining the tilt angle.

Holes

The holes are certainly located close to *T*, the center of the hexagonal face, and are very probably in a single

[15] The reciprocal masses were calculated from Berlincourt's masses. There is some uncertainty in the matrix inversion because the determinant is very small.

[16] A. L. Jain and S. H. Koenig, Phys. Rev. **127**, 442 (1962).
[17] D. Weiner, Phys. Rev. **125**, 1226 (1962).
[18] L. C. Hebel and P. A. Wolff, Phys. Rev. Letters **11**, 368 (1963), and many references cited in this letter and in Ref. 17.

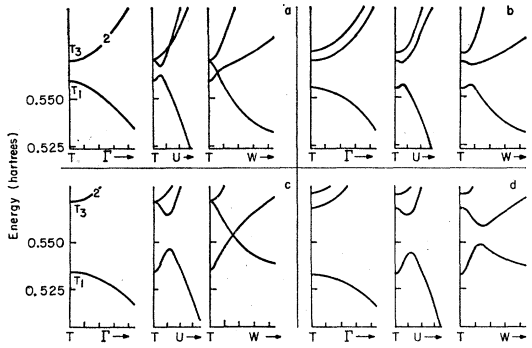

FIG. 5. Details of the band structure close to T (holes). (a) Pseudopotential $P1$ without spin; (b) pseudopotential $P1$ with spin-orbit coupling included; (c) pseudopotential $P8$ without spin; (d) pseudopotential $P8$ with spin-orbit effects. The divisions in the abscissae indicate 1/10 of the distance between T and the corresponding end point (Γ, U, or W).

pocket centered at T.[19] The proximity of the T_1 and T_3 levels, the degeneracy of T_3 and the crossover degeneracy along TW, required by the compatibility relations, make the introduction of spin-orbit coupling necessary to understand the details of the hole surface. However as it is evident from Fig. 3 and Figs. 5(a), (c), before spin-orbit effects are included the T-U and T-W show very different band structures. This makes the singly connected "ellipsoid" very warped. The warping should show very clearly in the dH–vA oscillations when the magnetic field is rotated in a plane perpendicular to the trigonal axis. Berlincourt[12] performed this experiment but his results are inconclusive: the amplitudes of the oscillations, when measured by the torque method, are very weak for these orientations. Further discussion of the hole pocket is left for Sec. 6.

6. THE SPIN-ORBIT EFFECTS

The spin-orbit coupling has been included in the calculation *a posteriori*, by means of an approximate perturbation approach and only in the neighborhood of the points T and L, where it may be of importance.

As is well known, the spin-orbit splitting at the top of the valence band in germanium ($Z=32$) amounts to 0.29 eV $\cong$0.01 hartree[20] and is, of course, smaller than the typical band gaps due to the crystal potential. The splitting quoted above is also to be compared with the "atomic" spin-orbit splitting which in Ge II amounts to 0.22 eV between the $J=\frac{1}{2}$ and $J=\frac{3}{2}$ lines of the $4p\,^2P$ ground state.[21]

In arsenic, the nearest neighbor to the right of germanium in the periodic table, the corresponding splitting ($J=\frac{1}{2}$ and $J=\frac{3}{2}$ in the $4p\,^2P$ ground state of As III) is 0.36 eV.[21] On the other hand the crystal structure of As is only rhombohedral while Ge is cubic and the spin splitting in a rhombohedral system is only about $\frac{2}{3}$ as large as the splitting in the corresponding cubic structure. Consequently, by putting all these pieces of information together, arsenic is expected to have, at the points of higher symmetry (Γ, T or Λ), a maximum spin splitting of about 0.24−0.32 eV, i.e., of the order of 0.01 hartree. The effect, as expected, is small and can be of importance only at places of degeneracy or near degeneracy (e.g., T and L) where the new splittings may change ordering of levels and connectivity of lines.

We have chosen to include spin-orbit effect by means of a "tight-binding" approach which can be considered accurate to better than a factor of 2; for such a small effect the errors involved are not very important and any more accurate calculation would involve a major change in the computational technique as well as much more running time in the computer. It may be noted in passing that such a modification of the computational approach is an absolute necessity in bismuth, where spin-orbit gaps ($\sim$1.5 eV) are probably larger than most crystal-potential gaps; the situation in antimony (spin gaps of about 0.6 eV) is intermediate between the As and Bi cases.

For the calculation of the spin-orbit effects in arsenic the following approximations are made:

(a) The actual crystal potential (not the pseudopotential in this case) is assumed to be spherically symmetric about each ion and constant in the region between ions;

(b) The actual conduction electron wave functions (not the smooth part of them) are assumed to have a definite angular-momentum character (s, p, d, etc.) about each ion; for the first few bands and close to the ions they are supposed to behave like the atomic $4s$ and $4p$ functions.

(c) The atomic-like character of a given energy level in the neighborhood of a given symmetry point, say T or L, is supposed to be identical with the character *at* the symmetry point; in case of degeneracy group-theoretical considerations indicate the right choice of symmetry.

Assumptions (a) and (b) permit one to write the usual spin-orbit Hamiltonian[22]

$$\mathcal{H}_{so}=\frac{1}{2mc^2}(\nabla V\times\mathbf{p}\cdot\mathbf{S}) \tag{6.1}$$

in the simplified form equal to

$$\mathcal{H}_{so}=\lambda\sum_{\alpha,\text{ ion sites}}\mathbf{L}_\alpha\cdot\mathbf{S} \tag{6.2}$$

when dealing with the first few bands of the structure.

In (6.2) $\mathbf{L}_\alpha$ is an angular momentum operator which

[19] Also conceivable are six equivalent pockets in the hexagonal face or two equivalent pockets in the Λ line close to T.

[20] See for instance C. Kittel, *Quantum Theory of Solids* (John Wiley & Sons, Inc., New York, 1963), p. 276.

[21] C. E. Moore, Natl. Bur. Std. Circ. 467 (1949).

[22] R. J. Elliott, Phys. Rev. **96**, 280 (1954).

acts only on "atomic-like" functions centered around site α, and λ is chosen in such a way that the expectation value of $\mathcal{H}_{so}$ for $(4p, J=\frac{3}{2})$ and $(4p, J=\frac{1}{2})$ wave functions reproduces the observed atomic splitting $\Delta_{at}=0.364$ eV $=0.0135$ hartree, namely $\lambda=0.009$ atomic units.

In regard to the angular-momentum character of the wave functions, crystal chemistry considerations[7] as well as detailed analysis show that close to the Fermi energy the p-like character should dominate and for, *spin-splitting analysis*, a *tight-binding approach* should in fact give fairly good answers.

If we now restrict our attention to the T and L levels (and in particular to T_1, T_3, L_1, and L_4 symmetries) and their neighborhoods, group-theoretical considerations obtained from Tables II through VII indicate:

(a) The following set of levels,

(1) $T_1T_2T_3$,
(2) $T_1'T_2'T_3'$,
(3) L_1L_2,
(4) L_3L_4,

interact via spin-orbit coupling within each set but not between different sets.

(b) The level T_1, and the Λ_1, Q_1, and M_1 levels compatible with it, behave close to the ions like p functions parallel to the trigonal axis.

(c) One of the T_3 levels, one of the Λ_3 levels and the Q_2 and M_2 levels connected to T_3 behave close to the ions like p functions parallel to the binary axis.

(d) The second T_3 level, the second Λ_3 level and the Q_1 and M_1 levels connected to T_3 behave close to the ions like p function perpendicular to both the binary and the trigonal axes.

(e) The L_1 levels behave close to the ions like p functions perpendicular to the binary axis.

For the actual calculation all these properties are taken into account and use is made of the well-known matrix elements of the operator $\mathbf{L}\cdot\mathbf{S}$ between any two p functions of either spin.

For the point T and its neighborhood we have only considered the T_1 and T_3 levels. The resulting 6×6 matrix to be diagonalized can be immediately factorized into two identical 3×3 matrices:

$$\begin{vmatrix} E_1(\mathbf{k}) & -\lambda & i\lambda \\ -\lambda & E_2(\mathbf{k}) & i\lambda \\ -i\lambda & -i\lambda & E_3(\mathbf{k}) \end{vmatrix}, \tag{6.3}$$

where $E_1(\mathbf{k})$ represents the T_1 (Λ_1, M_1 and Q_1) energy, $E_2(\mathbf{k})$ is the T_3 (Λ_3, M_2 and Q_2) energy and $E_3(\mathbf{k})$ gives the energy of T_3 (Λ_3, M_1 and Q_1), all of them in the absence of spin-orbit coupling. The eigenvalues of (6.3) are plotted in Fig. 5 for two pseudopotentials. In Figs. 5 (a) and (b) the $E(\mathbf{k})$ correspond to pseudopotential $P1$, and in (c) and (d) to pseudopotential $P8$; (a) and (c) correspond to $\lambda=0$ and (b) and (d) to $\lambda=0.009$.

The point L was treated in a similar manner, restricting the calculation to the (L_1, L_1, L_4) triplet. Since L_1 and L_4 do not interact, the secular equation is reduced in this case to a 2×2 problem. It should be noted that, if in the absence of spin the L_4 level lies between the two L_1 levels [as in Fig. 4(c) for pseudopotential $P8$], there is an accidental crossover of bands close to L and along the L-W line between a Q_1 and a Q_2 symmetry. Table V shows that such a crossover should be removed by spin-orbit coupling although our approximate method of calculation yields no lifting of this degeneracy. The degeneracy is indeed removed, but the gap should be at least one order of magnitude smaller than the other spin-orbit gaps. It is proportional to the amount of mixing of symmetric and antisymmetric character in the wave function at this point in k space. Close to L the amount of mixing should indeed be small. The removal of the degeneracy is indicated qualitatively in Fig. 4(d).

Analysis of the results shown in Fig. 4 indicate that for L no important changes due to spin-orbit coupling appear in the band structure. The only relevant results seem to be an additional "repulsion" of the two L_1 levels and the appearance of a very small energy gap at the possible accidental degeneracies. The analysis of the electron surfaces carried in the last section is therefore essentially unchanged.

The band structure close to T (Fig. 5) on the contrary, is profoundly altered by spin effects and on the whole tends to be much simpler, with all the degeneracies eliminated. This will tend to make the hole portion of the Fermi surface less "anisotropic" than the no-spin bands would suggest. Figure 5(b), which we believe closer to the actual band structure, gives rise to a prolate "ellipsoid," fairly "isotropic" normal to trigonal axis; the trigonal effective mass is in this case larger (in absolute value) than the perpendicular mass. However the "anisotropic" possibilities are not completely removed, as the example of pseudopotential $P8$ [Fig. 5(d)] shows. Although we do not believe this to be the actual case, in arsenic this kind of irregular band structure should be kept in mind when trying to explain the irregular behavior of some alloys of the semimetals.[1]

In conclusion we would like to extrapolate the results obtained here to the other semimetals, Sb and Bi.[1,23] Sb seems to have a set of three ellipsoids which roughly fits the tilt angle corresponding to the X_1 level (sixth band at X); it may also have another set of electron pockets at or near L which would be nonellipsoidal.

Bi has definitely a set of three equivalent electron pockets of nonellipsoidal nature arising from nonparabolic bands. If the over-all band structure resembles that in arsenic and inclusion of the large spin-orbit

[23] J. J. Hall and S. H. Koenig, IBM J. Res. Develop. 8, 241 (1964), and the references there quoted.

effects does not change it drastically, the electrons should be located at L, as has been previously suggested.[23]

ACKNOWLEDGMENTS

We would like to acknowledge several discussions with Morrel H. Cohen, J. Ketterson, and P. M. Lee.

We are grateful to the National Science Foundation and the U. S. Office of Naval Research for direct financial support of this work. In addition the research benefited from partial support of related solid-state theory by the National Aeronautics and Space Administration and general support of the Institute for the Study of Metals by the Advanced Research Projects Agency and the National Science Foundation.

APPENDIX A: DETAILS OF THE CRYSTAL STRUCTURE

Figure 6 shows the Brillouin zone of arsenic and the rhombohedron of twice the volume, from which it is obtained. The rhombohedron is the Brillouin zone in the absence of internal displacement, i.e., $u=0.25$. The axes labeled x, y, z are the cubic axes in the absence of shear and it is convenient to keep them as an orthogonal system of coordinates. The three primitive translation vectors of the As lattice can then be expressed by

$$\begin{aligned}\mathbf{a}_1&=a_0\{\epsilon,1,1\},\\ \mathbf{a}_2&=a_0\{1,\epsilon,1\},\\ \mathbf{a}_3&=a_0\{1,1,\epsilon\},\end{aligned}\tag{A1}$$

where { } indicate rectangular coordinates.

Values of $|\mathbf{a}_i|$, a_0, and ϵ are given in Table I. The parameter ϵ is related to the shear angle α by

$$\cos\alpha=(1+2\epsilon)/(2+\epsilon^2)\tag{A2}$$

$$\epsilon=[1-(1+\cos\alpha-2\cos^2\alpha)^{1/2}]/\cos\alpha.\tag{A3}$$

α is the angle between any two $\mathbf{a}_i$. No shear implies $\alpha=60°$, $\epsilon=0$ and the $\mathbf{a}_i$'s become the primitive translations of the face-centered cubic lattice.

The three reciprocal lattice vectors defined by

$$\mathbf{g}_i\cdot\mathbf{a}_i=2\pi\delta_{ij}$$

are given by

$$\begin{aligned}\mathbf{g}_1&=g_0\{-(1+\epsilon),1,1\},\\ \mathbf{g}_2&=g_0\{1,-(1+\epsilon),1\},\\ \mathbf{g}_3&=g_0\{1,1,-(1+\epsilon)\},\end{aligned}\tag{A4}$$

where g_0 is listed in Table I. A general reciprocal lattice vector is indicated by

$$[h,k,l]\equiv h\mathbf{g}_1+k\mathbf{g}_2+l\mathbf{g}_3,\tag{A5}$$

where h, k, l are integers; similarly, points in the Brillouin zone or in reciprocal space in general are denoted by

$$[a,b,c]\equiv a\mathbf{g}_1+b\mathbf{g}_2+c\mathbf{g}_3.\tag{A6}$$

The symmetry points in the Brillouin zone shown in Figs. 1 and 6 are

$$\begin{aligned}&\Gamma=[0,0,0], && T=[\tfrac{1}{2},\tfrac{1}{2},\tfrac{1}{2}],\\ &X=[0,\tfrac{1}{2},\tfrac{1}{2}], && W=[\gamma,1-\gamma,\tfrac{1}{2}],\\ &L=[0,\tfrac{1}{2},0], && U=[\tfrac{1}{2}\gamma+\tfrac{1}{4},1-\gamma,\tfrac{1}{2}\gamma+\tfrac{1}{4}],\\ &L'=[-\tfrac{1}{2},0,0], && K=[0,\tfrac{3}{4}-\tfrac{1}{2}\gamma,\tfrac{1}{2}\gamma+\tfrac{1}{4}],\end{aligned}$$

where

$$\gamma=(1+\tfrac{1}{2}\epsilon^2)/(2+\epsilon)^2=0.2303.$$

The following angles between the faces of the Brillouin zone of interest:

(a) Angle between hexagonal (T) and rectangular (X) faces, 120° 43′,

(b) Angle between pseudohexagonal (L) and rectangular (X) faces, both adjacent to same hexagonal face, 124° 10′,

(c) Angle between pseudohexagonal (L') and rectangular (X) faces not adjacent to same hexagonal face, 131° 07′,

(d) Angle between hexagonal (T) and pseudohexagonal (L) faces, 107° 10′,

(e) Angle between two adjacent pseudohexagonal (L, L') faces, 111° 40′.

In the absence of shear the first three angles are equal to 125° 16′ and the last two equal to 109° 28′.

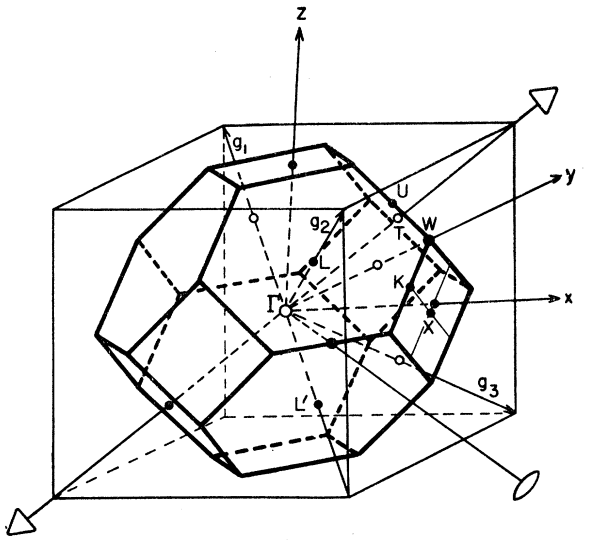

FIG. 6. The Brillouin zone for arsenic inscribed in the rhombohedron corresponding to the Brillouin zone of the simple-rhombohedral structure. Trigonal and binary axes are indicated as well as the rectangular system of coordinates xyz used in the initial calculations. Primitive reciprocal lattice vectors $\mathbf{g}_1\mathbf{g}_2\mathbf{g}_3$ of the A7 structure are also shown.

APPENDIX B: THE SYMMETRIZED COMBINATIONS OF PLANE WAVES

Symmetrized combinations of plane waves can be obtained by means of the character tables of Sec. 3.

TABLE X. Coefficients of the symmetrized combinations of plane waves at Γ and T.

k vector[e]	Γ_1 T_1	Γ_1' T_1'	Γ_2 T_2	Γ_2' T_2'	Γ_3A[f] T_3A	Γ_3B[f] T_3B	$\Gamma_3'A$[f] $T_3'A$	$\Gamma_3'B$[f] $T_3'B$
$[0, 0, 0]$[a]	1							
$[a, a, a]$[b]	1			1				
$[-a, -a, -a]$	1			−1				
$[a, b, b]$[c]	1			1	2	0	0	2
$[b, a, b]$	1			1	−1	−1	1	−1
$[b, b, a]$	1			1	−1	1	−1	−1
$[-a, -b, -b]$	1			−1	2	0	0	−2
$[-b, -a, -b]$	1			−1	−1	−1	−1	1
$[-b, -b, -a]$	1			−1	−1	1	1	1
$[0, -a, a]$[a,b]	1	1			2	0	2	0
$[a, 0, -a]$	1	1			−1	−1	−1	−1
$[-a, a, 0]$	1	1			−1	1	−1	1
$[0, a, -a]$	1	−1			2	0	−2	0
$[-a, 0, a]$	1	−1			−1	−1	1	1
$[a, -a, 0]$	1	−1			−1	1	1	−1
$[a, b, c]$[d]	1	1	1	1	2 0	2 0	2 0	2 0
$[c, a, b]$	1	1	1	1	−1 1	−1 −1	−1 1	−1 −1
$[b, c, a]$	1	1	1	1	−1 −1	−1 1	−1 −1	−1 1
$[a, c, b]$	1	−1	−	1	2 0	−2 0	−2 0	2 0
$[b, a, c]$	1	−1	−1	1	−1 1	1 −1	1 1	−1 1
$[c, b, a]$	1	−1	−1	1	−1 −1	1 1	1 −1	−1 −1
$[-a, -b, -c]$	1	−1	1	−1	2 0	2 0	−2 0	−2 0
$[-c, -a, -b]$	1	−1	1	−1	−1 1	−1 −1	1 −1	1 1
$[-b, -c, -a]$	1	−1	1	−1	−1 −1	−1 1	1 1	1 −1
$[-a, -c, -b]$	1	1	−1	−1	2 0	−2 0	2 0	−2 0
$[-b, -a, -c]$	1	1	−1	−1	−1 −1	1 −1	−1 −1	1 −1
$[-c, -b, -a]$	1	1	−1	−1	−1 1	1 1	−1 1	1 1

[a] T has no k vectors of this form.
[b] $a \neq 0$.
[c] $a \neq b$.
[d] $a \neq b \neq c$; if $a=0$, then $|b| \neq |c|$ (and similarly if b or $c=0$).
[e] Form of $\mathbf{k}-\mathbf{G}$, where $\mathbf{k}=\Gamma$ or T and $\mathbf{G}$ is a reciprocal lattice vector.
[f] A and B correspond to different rows of the two-dimensional representation and are degenerate in the case of no spin. Note also that two different linear combinations of vectors $[a, b, c]$ belong Γ_3A and Γ_3B. Both must be used in a calculation.

TABLE XI. Coefficients of the symmetrized combinations of plane waves at Λ.

k vector[a]	Λ_1	Λ_2	Λ_3A[b]	Λ_3B[b]
$[a, a, a]$	1			
$[a, b, b]$	1		2	0
$[b, a, b]$	1		−1	−1
$[b, b, a]$	1		−1	1
$[a, b, c]$	1	1	2 0	2 0
$[c, a, b]$	1	1	−1 1	−1 −1
$[b, c, a]$	1	1	−1 −1	−1 1
$[a, c, b]$	1	−1	2 0	−2 0
$[b, a, c]$	1	−1	−1 −1	1 −1
$[c, b, a]$	1	−1	−1 1	1 1

[a] Form of $\mathbf{k}-\mathbf{G}$, where $\mathbf{k}=\Lambda$ ($\Lambda=[\delta, \delta, \delta]$; $0<\delta<\frac{1}{2}$) and $\mathbf{G}$ is a reciprocal lattice vector.
[b] See footnote f of Table X.

TABLE XII. Coefficients of the symmetrized combinations of plane waves at X and L.

k vector[c]	X_1 L_1	X_2 X_2	X_3 L_3	X_4 L_4
$[a, b, b]$	1			1
$[-a, -b, -b]$	1			−1
$[0, a, -a]$[a]	1		1	
$[0, -a, a]$	1		−1	
$[a, b, c]$[b]	1	1	1	1
$[a, c, b]$	1	−1	−1	1
$[-a, -b, -c]$	1	1	−1	−1
$[-a, -c, -b]$	1	−1	1	−1

[a] L has no k vectors of this form.
[b] $b \neq c$; if $a=0$ then $|b| \neq |c|$.
[c] Form of $\mathbf{k}-\mathbf{G}$, where $\mathbf{k}=X$ or L ($X=[0, \frac{1}{2}, \frac{1}{2}]$; $L=[\frac{1}{2}, 0, 0]$) and $\mathbf{G}$ is a reciprocal lattice vector.

However, if complete factorization for the doubly degenerate levels is needed, the complete matrix representations rather than the character tables are necessary. In Tables X–XII we give complete factorizations for the points Γ, T, Λ, X, and L. The other points are trivial. The tables list the k vectors of the plane waves in trigonal notation (A6). The coefficients are not in normalized form.